Thermal Diffusivity Measurements of Oxide and Metallic Melts at High Temperature by the Laser Flash Method

Yoshio Waseda, Hiromichi Ohta*, Hiroyuki Shibata and Tsuyoshi Nishi

Institute of Multidisciplinary Research for Advanced Materials, Tohoku University, Sendai 980-8577, Japan.
** Department of Materials Science, Faculty of Engineering, Ibaraki University, Hitachi 316-8511, Japan.*
e-mail: waseda@tagen.tohoku.ac.jp

(Received February 20, 2003; final form March 14, 2003)

ABSTRACT

An attempt has been made to describe the current status on thermal diffusivity measurement of oxide and metallic melts by the laser flash method in the temperature range between 1000 and 2000 K. This paper is to provide the principle and the new data processing for the laser-flash methods, including some selected examples of their application in determining thermal diffusivity of oxide and metallic melts at high temperature.

To overcome experimental difficulties at high temperature, a differential scheme without information of the absolute value of sample thickness was used in the oxide melt case with the help of a numerical technique to estimate the effect of radiative heat transfer in the cell system where the absorption and emission behavior of the radiative component in the sample layer were considered. For metallic melts, a new simple cell system was developed to keep a precise value of sample thickness and the effect of conductive or radiative heat leak from sample was also taken into account.

1. INTRODUCTION

Heat transfer property such as thermal diffusivity of high temperature melts with sufficient reliability is essential in order to design various manufacturing plants. This includes molten iron at elevated temperature and continuous casting powder melts consisting of various oxide components; SiO_2, Al_2O_3, MgO, CaO, etc. for further improving the present continuous casting process for steel /1/. However, thermal diffusivity measurements of high temperature melts are still far from complete in various cases, arising mainly from onset convective heat flow, heat leakage to the container and mixed contributions of radiative and conductive heat transfer components.

Thus, the available thermal diffusivity values of high temperature melts, compiled in the TPRC handbook /2/, frequently induce differences between the simulated results and experimental data, because almost all values in the TPRC handbook are estimated from the measured values of respective substances in the solid states.

In producing single crystals supplied for devices of semiconductor compounds in groups III through V such as GaAs and GaP, for example using the Czochralski method, the components of high vapor pressure such as P and As are likely to diffuse from the master melt, causing the original compositions to change. In order to reduce such problems, boron oxide melts have recently been widely used as liquid capsules to encase molten semiconductors. In order to obtain high quality single-crystal semiconductors with a low dislocation density, it is necessary to minimize the temperature gradient in the melt by accurate temperature control. For this purpose, the thermal diffusivity of a liquid capsule material is one of the important properties. Nevertheless, no report is available on the thermal diffusivity of molten boron oxide within the best knowledge of the present authors.

On the other hand, the laser flash method, first proposed by Parker and his colleagues/3/, is widely employed as one of the most versatile techniques for measuring thermal diffusivity of various materials. Particularly, a three layered cell by the laser flash method has been successfully developed for determining the thermal diffusivity of high temperature melts of both oxides and metals /4-6/.

The main purpose of this work is to describe the current state-of-the-art concerning the laser flash method with some selected examples of the thermal diffusivity values of high temperature melts by precisely separating the radiative component from measured values.

2. EXPERIMENTAL PROCEDURES AND THEORETICAL BASIS

The laser flash apparatus for measuring thermal diffusivity of various substances has already been described /3,7/ and one example is shown in Fig. 1 using the schematic diagram of the experimental arrangement in the vertical line-up. The front surface of a sample is irradiated by a ruby (or Nd glass) laser beam with a pulse duration of the order of 1 ms and the temperature response at the back surface of the sample is measured by using an InSb infrared detector (1.2-5.5 μm effective wavelength). The sample is usually heated up to the desired temperature, within ±2 K controlled by a thermocouple installed near the sample cell, using an additional heating element such as a tungsten mesh heater under vacuum of less than 2 x 10^{-3} Pa and a platinum coil heater under the air atmosphere.

The three layered cell assembly for oxide melts is given in Fig. 2 /5/. A platinum crucible containing a small amount of a liquid sample is placed on the alumina pipe. The crucible size (corresponding to the third layer) is 0.2 mm thick, 10 mm deep and 19 mm in diameter. Another relatively small platinum crucible of 0.2 mm thickness, 10 mm depth and 14 mm diameter is used as the first layer and it is centered to the end of the alumina tube by ceramic cement. The alumina tube is connected to a holder on a three axial movable arm and the top platinum crucible is located right above the bottom one to consist of a three layered cell. The crucible size depends on the materials of interest. A typical flow of a measuring process is as follows.

The inner and outer platinum crucibles were

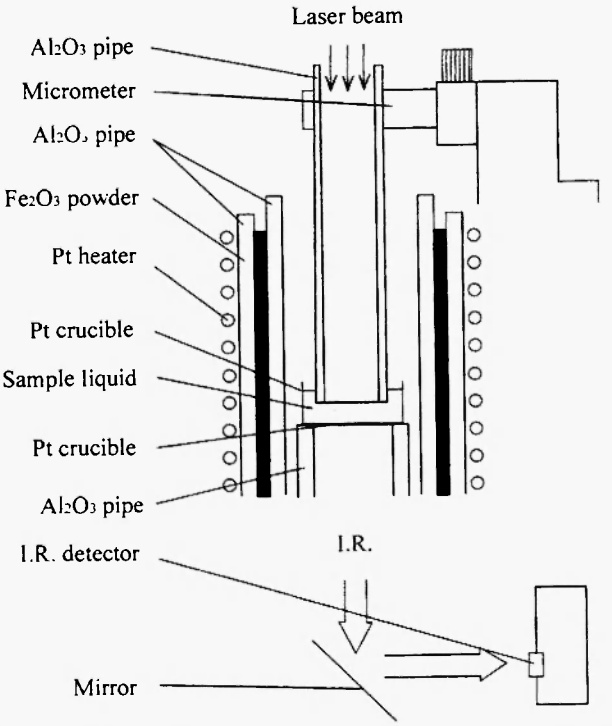

Fig. 1: Schematic diagram of a laser flash apparatus at high temperature.

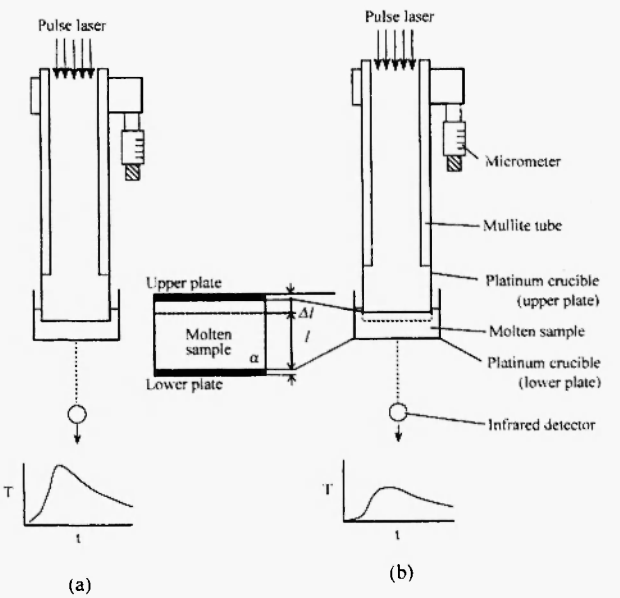

Fig. 2: Schematic diagram of the cell system for oxide melts in the three layered laser flash method.

separated several times during the course of the experiments to check that there was no bubble in a liquid sample. The alumina pipe was lowered vertically by a micrometer. Then, a laser pulse was flashed on the top surface of the inner crucible (the first layer). The temperature response curve was recorded by means of an infrared detector focused on the back surface of the outer crucible (the third layer) through a gold mirror. Another temperature response curve was also measured after changing the thickness of a liquid sample. The variation of the sample thickness can be determined by reading a micrometer scale attached on the holder. In this work, the relative difference of sample thickness Δl in two sets of the measurements was fixed to be 0.2 mm, on the basis of the previous results on high temperature melts using the three layered laser flash method /5,6/. After measurement, the upper platinum crucible was raised to again check visually that there were no bubbles in the sample. From the results of measurement using the three layered cell filled with distilled water, and molten carbonate salts, it was found that the experimental uncertainties were within ± 5 % of the literature values.

An easy and reliable data processing method has been developed to estimate the thermal diffusivity of a liquid sample at high temperature using the three layered laser flash method /4/. This is based on a point that the initial time region of the temperature response curves is unlikely to be affected by heat loss by conduction from the sample to the holder and by radiation. Only the essential points are given below for convenience of discussion.

The temperature response of the three layered cell at the initial time region of the temperature response curve can be expressed in the following form, analogous to the approach for a two layered cell proposed by James /8/.

$$\frac{\partial \ln(T\sqrt{t})}{\partial(1/t)} = -\frac{(\eta_1 + \eta_2 + \eta_3)}{4} \qquad (1)$$

where η_i is $l_i\sqrt{\ }$, T is temperature rise and t is time after irradiating a laser pulse.

The thickness and thermal diffusivity of the i-th layer are denoted by l_i and α_i, respectively. Thus, a plot of $\ln(\ln(T\sqrt{\ }))$ against $1/t$ for Eq. (1) gives a straight line with slope of $-(\eta_1+\eta_2+\eta_3)^2/$. The thermal diffusivity value of α_2 of the second layer (a melt sample in the present case) can readily be estimated, when the thermal diffusivity values of the first and third layers (platinum in the present case) and the thickness of all three layers are given.

Let us consider an infinite slab as shown in Fig. 2 consisting of three layers. At the initial time region, the temperature response of the back surface of the third layer can be described as Eq. (1). Then, we can obtain the following relations:

$$l_2/\sqrt{\alpha_2} = 2\sqrt{-\frac{\partial \ln(T_{(l_2)}\sqrt{t})}{\partial(1/t)}} - \eta_1 - \eta_2 \qquad (2)$$

$$(l_2 + \Delta l)/\sqrt{\alpha_2} = 2\sqrt{-\frac{\partial \ln(T_{(l_2+\Delta\eta)}\sqrt{t})}{\partial(1/t)}} - \eta_1 - \eta_2 \qquad (3)$$

Here, l_2 is the thickness of a melt sample in the first measurement and Δl is the relative change of sample thickness corresponding to the difference between two measurements produced by lifting up the inner crucible (the first layer in the present case).

The relation between the sample thickness l_2 and the sample thermal diffusivity α_2 is described as a solid line in Fig. 3 /5/. For a given Δl, the similar relation between l_2 and $l_2 + \Delta l$ is also given as a dashed line in Fig. 3. The intersection of these two lines provides the resultant thermal diffusivity value of a melt sample α_2 and its thickness l_2. In practice, a curve fitting procedure using the time region in the range 0.2 and 0.4 t_{max} is usually

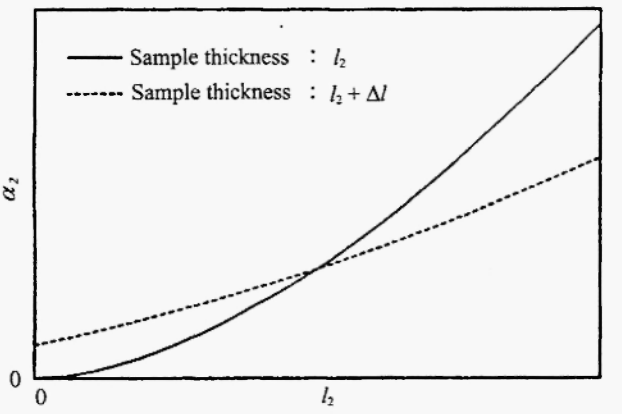

Fig. 3: Relationship of α_2 as a function of thickness estimated from eqs. (2) and (3).

used. The essential points are as follows. The temperature response curve is estimated at one thickness l_2 as shown schematically in Fig. 4(a) and values of θ obtained at t_a and t_b. The same procedure is utilized using the time region for a thickness $l_2 + \Delta l$. The two response curves are converted as provided in Fig. 4(b) and the respective gradients β_1 and β_2 are estimated by the least squares method. A value is selected for l_2 and an approximate α_2 value calculated for each case. Then, this value is put into the thermal diffusion equation, and, using Laplace transformation and then inverse Laplace transformation, values of β_{LAP1} and β_{LAP2} are computed. By successive approximations, the α_2 values for two cases can be obtained that satisfy the relation of $\beta_1 = \beta_{LAP1}$ and $\beta_2 = \beta_{LAP2}$. By iteration with different values of l_2, the α_2 values are evaluated in order to provide a temperature response curve of $l_2 + \Delta l$, from which a final value of α_2 can be obtained from the intersection of the two curves. More detailed information for this data processing is given in ref.5.

It may also be worth mentioning that, from recent simulated results using the finite element method, the heat leakage through a side wall of a platinum crucible is able to reduce less than 5 %, when only the values of sample thickness and its variation are carefully selected /5,9/. Also, from the results of systematic measurement with samples having different diameters larger than that of the laser beam, it was proved that the shape of the three layered cell presently used reduces heat leakage to the sample container and the radial heat flow was confirmed to be insignificant /4-6/.

On the other hand, another three layered cell has been developed for keeping the shape of metallic melt uniform for a given thickness. A schematic diagram of the devised cell is shown in Fig. 5 /10/. This cell system consists of ceramic (alumina or mullite) tube and two sapphire plates; sapphire is known to be transparent for ruby or Nd glass laser and infrared ray. In other words, alumina or mullite tube is sandwiched between two sapphire plates. The advantage of this sample cell is to vary the sample thickness easily by changing the thickness of the ceramic tube, depending upon thermophysical properties of the desired sample. Four

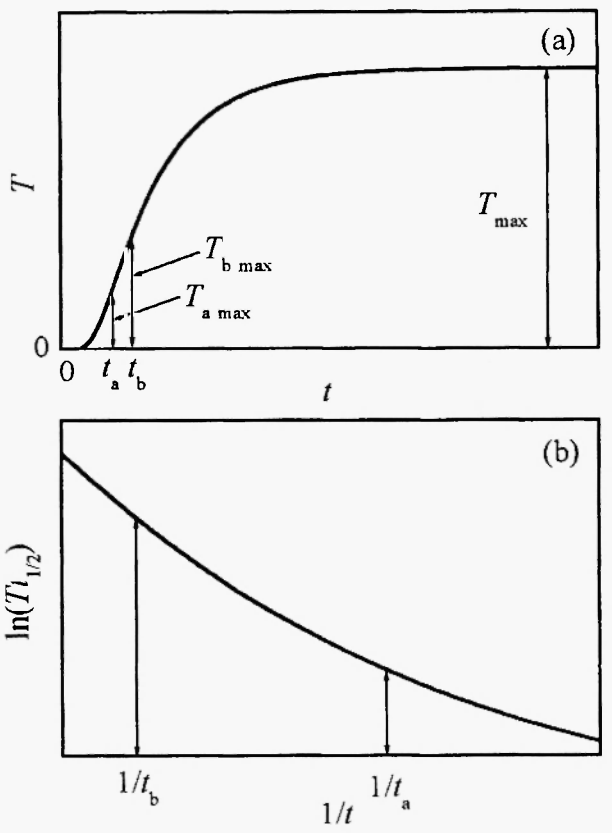

Fig. 4: Principle of data processing from experimental output of T vs t. (a) Determination of t_a and t_b in the range 0.2 to $0.4T_{max}$. (b) Plot of $1/t$ vs $\ln(Tt_{1/2})$ to determine slopes β and β_2.

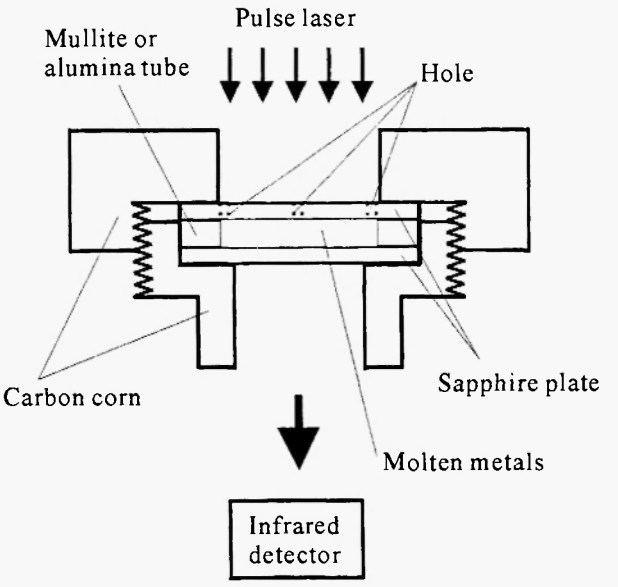

Fig. 5: Schematic diagram of the cell system for metallic melts in the three layered laser flash method.

small holes with size of 0.5 mm in diameter are made in the upper sapphire plate for reducing the volume expansion when the metal sample is melted and residual gas inside the sample. As shown in Fig. 5, this three-layered cell is fixed by the carbon corn. It is suggested that any leakage of molten metal from this cell system was not detected, probably because of relatively low wettability between molten metal and cell materials (alumina or mullite). The following comments may be worthy of note for further application of this type of cell.

Two kinds of sample cell systems were tested. One consists of a mullite tube (thickness: 0.8-1.5 mm, inner diameter: 9 mm, outer diameter: 13 mm) sandwiched by two sapphire plates (thickness: 1.0 mm, diameter: 13 mm). The other is a cell with an alumina tube (thickness: 0.8-1.5 mm, inner diameter: 9 mm, outer diameter: 13 mm) and two sapphire plates (thickness: 1.0 mm, diameter: 13 mm). The mullite tube cell was successively applied to the thermal diffusivity measurements of iron, cobalt and nickel. However, it should be kept in mind that mullite is not a suitable material to contain metallic melt at temperature above 1700 K for expected time span (about 3 hours). In the case of iron melt, we could not obtain a sufficiently reliable temperature response curve when using an alumina tube. This is considered mainly arising from a problem for alumina in degassing the residual gas inside the iron sample. In the cases of cobalt and nickel, there were no experimental problems associated with neither the mullite or alumina tubes /10/.

3. SELECTED EXAMPLES OF THERMAL DIFFUSIVITIES OF OXIDE MELTS

In producing single crystals of GaP using the Czochralski method, boron oxide is widely used as a liquid capsule material to encase molten semiconductors for reducing problems due to diffusion of high vapor pressure components. Thermal diffusivity data of boron oxide melt have been obtained by a three-layered laser flash method at intervals 50 to 100K over the temperature range of 1000 to 1500K /6/. Figures 6 and 7 indicate the results of boron oxide melts, with different water content, containing 0.08mol% In_2O_3 and molten

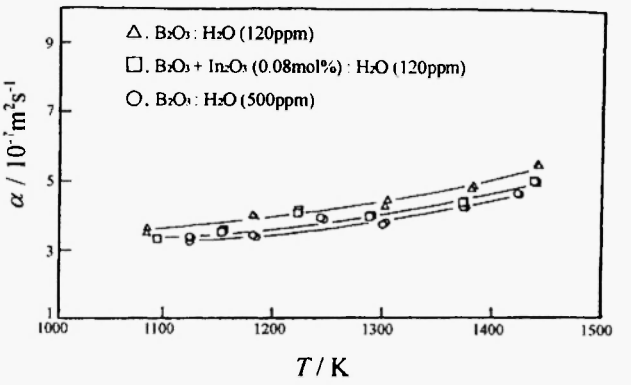

Fig. 6: Thermal diffusivity of molten boron oxide containing H_2O and In_2O_3 as a function of temperature.

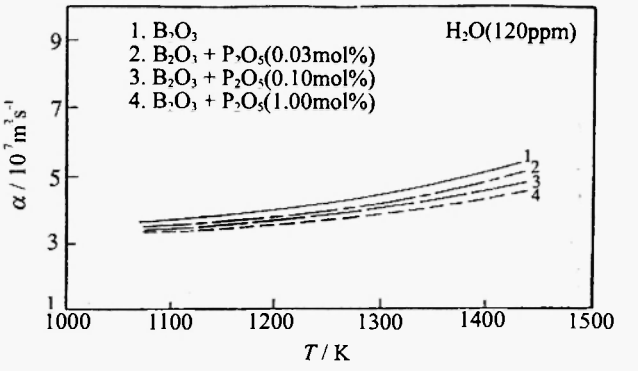

Fig. 7: Effect of the P_2O_5 content on thermal diffusivity of molten boron oxide (containing 120ppm water) as a function of temperature.

boron oxide containing a small amount of P_2O_5, respectively.

In all cases, the thermal diffusivity values of boron oxide melt increase with increasing temperature. Variations in thermal diffusivity, which are not prominent, systematically decrease as the contents of In_2O_3 and P_2O_5 increase. It can be qualitatively understood that the results are attributed to an increase of the disharmony of boron oxide melt resulting from the addition of another oxide, which causes the mean free path of phonons to decrease as compared with the values for pure boron oxide metals /10/, although some further studies are required to obtain the definite comments. It may also be noted that unless a forced dehydrating treatment such as bubbling is employed, the water content of the boron oxide melts does not change

even if samples are heated up to the temperature range of 1000 to 1500K.

The thermal diffusivity values of continuous casting powders for steel were systematically obtained by the three layered laser flash method /9/. The measured thermal diffusivity values are shown in Fig. 8(a) using the results of oxide melts containing titanium oxide and iron oxide as an example. Although there are differences in detail, similar results were obtained for 19 cases /9/. The results of Fig. 8(a) indicate a slightly positive temperature coefficient of thermal diffusivity of the continuous casting powder melts in the temperature range presently investigated. However, it should be mentioned that the present results are somewhat spread in certain temperatures and such scattering is considered beyond the experimental uncertainty. This is attributed to the effect of radiative heat transfer component in a melt. Although the initial time region of the temperature response curve is known not to be severely affected by the radiative heat transfer /8/, the radiative component should be separated from measured temperature response data. This is particularly true at higher temperatures.

Quantitative discussion of the radiative heat transfer in high temperature substances requires the absorption coefficient of samples of interest. The absorption coefficient data are considered to be essential for the semitransparent media, compared with the transparent and opaque cases. Figure 9 shows the absorption coefficients of three samples as a function of wave length together with that of the hemispherical emissive power of blackbody at 1573 K /12/. It is very interesting that the change in CaO/SiO_2 ratio or the addition of zirconium oxide and hafnium oxide to the reference composition (35.6% SiO_2, 19.9%, 17.1% CaF, 10.1% Na_2O, 9.3% MgO, 7.7% Al_2O_3 in mass %) appears not to vary significantly the absorption coefficient in the range between 1×10^{-6} and 4×10^{-6} m^{-1} /13/; the correction by the transparent body approximation is well accepted for these oxide samples with respect to the radiative heat transfer behavior. In other words, the contribution from the radiative component should be explicitly considered only for cases containing titanium oxide and iron oxide /12/.

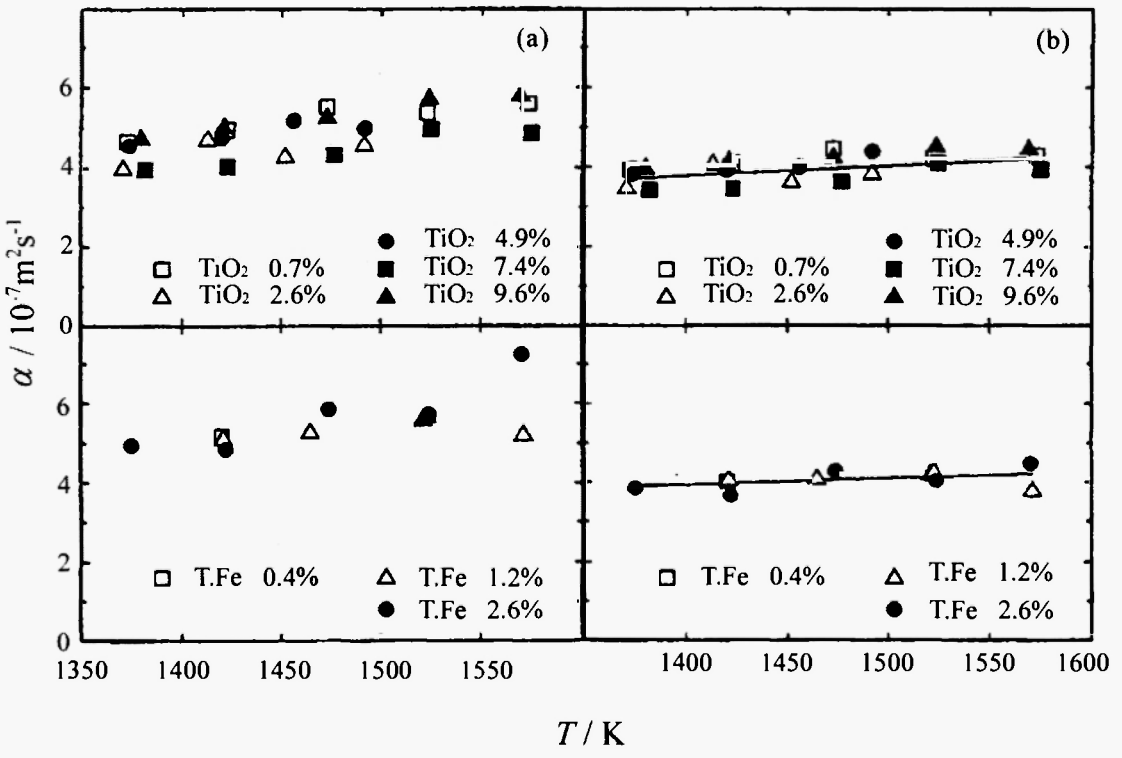

Fig. 8: Thermal diffusivity values of continuous casting powders for steel containing titanium oxide and iron oxide. (a) Radiative component is included, (b) Radiative component is excluded.

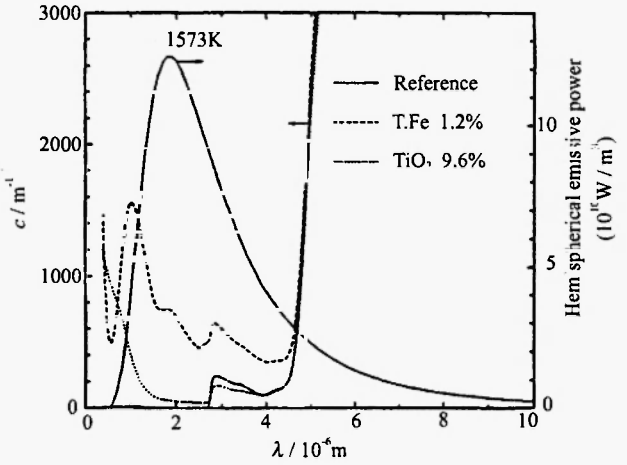

Fig. 9: Absorption coefficient of continuous casting powders for steel containing titanium oxide and iron oxide together with the hemispherical spectral emissive power of blackbody at 1573 K.

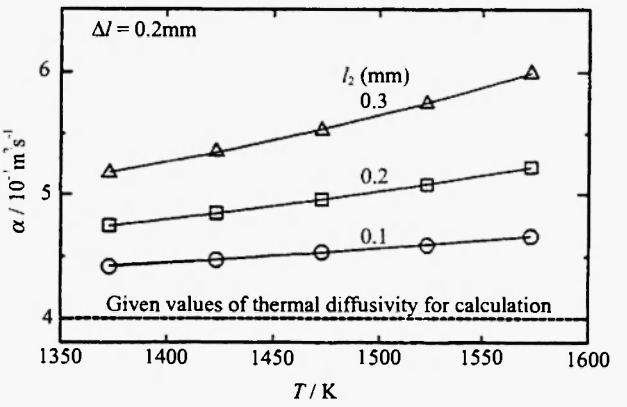

Fig. 10: Apparent thermal diffusivity indicating radiative heat flow theoretically calculated under the transparent body approximation for a sample of thermal diffusivity of 4 x 10^{-7} m^2/s.

When the transparent body approximation is valid, a liquid layer is considered to be transparent to radiative heat transfer where no radiation is absorbed or emitted from a liquid layer, and the radiation from a platinum plate is dominant. With respect to this subject, Ohta *et al.* /13/ have systematically estimated the effect of radiative component in the transparent body approximation by estimating the apparent thermal diffusivity values for a case of $\alpha_2 = 4\times10^{-7}$ m^2/s using the finite difference method in numerical calculation. The results are given in Fig. 10 and an essential point of these results indicates that the apparent thermal diffusivity values increase with increasing temperature and sample thickness by the contribution due to radiative component. These results also suggest that the radiative component induces an increase of about 20% in thermal diffusivity for the measurement where the sample thickness of 0.1 mm (for the first measurement) with its variation of 0.2 mm. The coefficients are summarized in the following form as a function of the absolute temperature T and the measured thermal diffusivity values should be corrected using these factors with the value of l_2.

$$\alpha = c\alpha_0 \tag{4}$$

$$\left.\begin{aligned} c &= 2.549\times10^{-7}T^2 - 4.504\times10^{-4}T + 1.244 \quad for\ l_2 = 0.1\,mm \\ c &= 6.986\times10^{-7}T^2 - 1.466\times10^{-4}T + 1.883 \quad for\ l_2 = 0.2\,mm \\ c &= 1.253\times10^{-6}T^2 - 2.675\times10^{-3}T + 2.606 \quad for\ l_2 = 0.3\,mm \end{aligned}\right\} \tag{5}$$

On the other hand, the absorption and emission of the radiative component in a liquid layer should be considered when the transparent body approximation is not well accepted as for a sample including iron oxide. Regarding this subject, fundamental equations have been given by considering all modes of radiative heat transfer /14/ and Ohta *et al.* /13/ reported the results of the gray body approximation where the spectral absorption coefficient of the semitransparent media is reduced to the mean absorption coefficient κ_m using Darby's equations coupled with the control volume method /15/. The temperature response is calculated as a function of κ_m and then the thermal diffusivity values can be obtained. The results are given in Fig. 11 for a case of thermal diffusivity of 4×10^{-7} m^2/s /13/. The validity and usefulness of these results may be confirmed by suggesting the following points. Good agreement is found with the value proposed by Rosseland /16/, who suggests for the condition of $\kappa l > 1$, in the higher absorption region larger than 10^5 m^{-1}. When the absorption coefficient is over 10^6 m^{-1}, it may be safely be said that samples are considered to be opaque and then the radiative contribution is

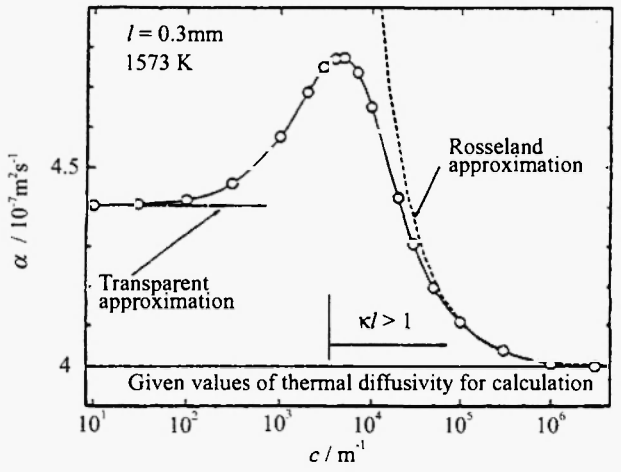

Fig. 11: Apparent thermal diffusivity including radiative heat flow theoretically calculated under the gray body approximation for a sample of thermal diffusivity of 4 x 10^{-7} m^2/s.

insignificant. On the other hand, in the lower absorption region less than 10^2 m^{-1}, the results are consistent with those of the transparent body approximation. The contribution from radiative component should be separated from the thermal diffusivity values experimentally determined using, at least, the gray body approximation or higher order (band) approximation in cases where the absorption coefficient is lying in the region between 10^2 and 10^4 m^{-1}. Samples containing titanium oxide and iron oxide are included in this category. Table 1 shows the mean absorption coefficient κ_m of samples containing titanium oxide and iron oxide

Table 1

Mean absorption coefficient κ_m for samples containing TiO_2 and iron oxide estimated from measured optical properties /12/.

Temperature (K)	1373	1473	1573
Type of Powder		κ_m	
Fe 0.4%	546	572	596
Fe 1.2%	774	810	844
TiO_2 2.6%	21	22	24
TiO_2 4.9%	39	41	43
TiO_2 9.6%	81	87	94

determined from the measurements of spectral transmissivity and reflectivity in the wave length region between 4×10^{-7} m and 1×10^{-5} m /11/.

Numerical estimation regarding the contribution of radiative component at high temperature measurements has been made using the three layered laser flash method /17/. In this work, the variation of the optical properties of samples is provided, and information about the apparent thermal diffusivity values is theoretically estimated for three cases of the transparent body approximation. The wave length dependence of the absorption coefficient, as exemplified by the results of Fig. 9, is explicitly included in the band approximation, although this requires lengthy numerical computation /13/. The theoretical details are given in /13/. The most significant aspects of this work are summarized in Table 2, providing the variation of the apparent thermal diffusivity values when using three different approximations for estimating the radiative contribution. The contribution from the radiative component could be estimated by the transparent body approximation with the experimental uncertainty less than 4% for samples recognized as transparent. However, the contribution from the radiative component should be estimated, at least, by the gray body approximation using the mean absorption coefficient for samples considered to be semi-transparent if we want to hold the experimental

Table 2

Apparent thermal diffusivity estimated from theoretical temperature response curves at 1575 K by the three layered laser flash method. Given thermal diffusivity: 4 x 10^{-7} m^2/s, sample thickness and its variation: 0.2 mm and 0.2 mm. The numerical values in the parenthesis correspond to the ratio of deviation from the case estimated under the band approximation /17/.

Type of powder	Approximation		
	Transparent	Gray	Band
Reference	4.90 (0.03)		5.05
Fe 0.4%	4.90 (0.09)	5.29 (0.02)	5.39
Fe 1.2%	4.90 (0.11)	5.44 (0.01)	5.50
TiO_2 2.6%	4.90 (0.04)	4.91 (0.04)	5.10
TiO_2 4.9%	4.90 (0.04)	4.93 (0.03)	5.11
TiO_2 9.6%	4.90 (0.05)	4.97 (0.03)	5.13

uncertainty down to less than 4%.

Based on these systematic results, the thermal diffusivity values were again estimated for continuous casting powders for steel by applying the transparent body approximation or the gray body approximation, depending upon the absorption coefficient behavior. The resultant thermal diffusivity values are illustrated in Fig. 8(b) using the results of samples containing titanium oxide and iron oxide. When comparing the results of Fig. 8(a), it is clearly found that scattering detected in measured values is considerably reduced by correcting the contribution from the radiative component, depending on both temperature and sample thickness. In addition, the thermal diffusivity values of continuous casting powders for steel are of the order to $4\pm0.5\times10^{-7}$ m^2/s and insignificant with the variation of temperature and concentration presently investigated.

4. SELECTED EXAMPLES OF THERMAL DIFFUSIVITIES OF METALLIC MELTS

Reliable values of thermal diffusivity of molten iron, cobalt and nickel at temperatures above 1700 K have recently been reported by using the laser flash method with a three layered cell /10/. In this work, the sample of metallic melts is held in a devised cell shown in Fig.5.

In the present experimental condition, it is necessary to consider the effect of not only radiative heat loss but also conductive heat loss at interface between metallic melt and cell material. Such information has recently been reported by Nishi *et al.* /10/ using numerical analysis with the following assumptions to construct the theoretical heat transport equation with the appropriate boundary conditions and the initial conditions.

(1) one dimensional heat flow,
(2) the whole cell is under adiabatic condition for the conductive heat flow,
(3) each layer is homogeneous,
(4) all thermophysical properties of the three layers are given,
(5) thermal contact resistance at the interface between layers is uniform and has same value at both the upper interface and the lower interface,
(6) heat pulse is uniformly absorbed on the front surface,
(7) radiative heat loss is proportional to the temperature difference, T_m T_e, where T_m is temperature increase of the metallic melt, T_e is steady-state temperature, respectively.
(8) no absorption of the energy in medium of the cell because the cell is transparent to both the laser pulse and infrared,
(9) radiative heat loss occurs only on the surface of the metallic melt.

The most important and significant points in their results are described below for further work on the thermal diffusivity measurements of metallic melts at high temperature. A typical temperature response curve where the dimensionless parameter of thermal contact resistance at interface, $R^* = \lambda_m R/l_m = 1$, and Biot number, $Y = 4\varepsilon\sigma T_e^3 l_m/\lambda_m = 0.$ is shown in Fig.12

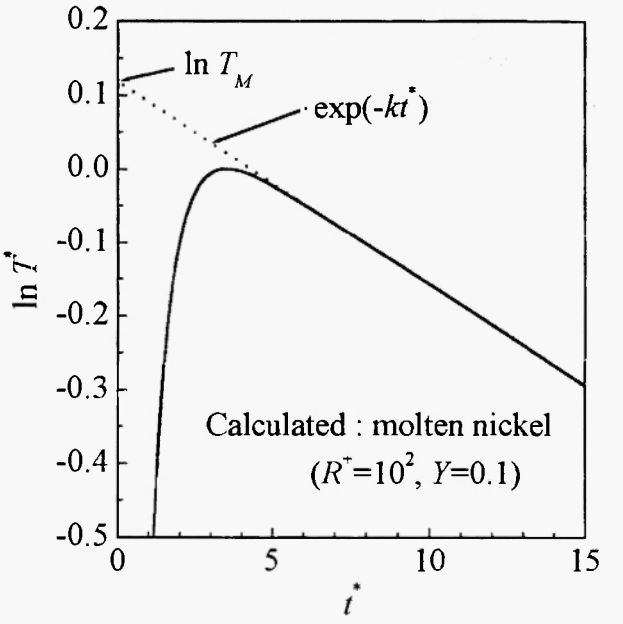

Fig. 12: Temperature response curve for molten nickel obtained by numerical simulation.

using the molten nickel case as an example, where λ_m is thermal conductivity of metallic melts, R is thermal contact resistance, l_m is sample thickness of metallic melts, ε is thermal emissivity of the surface of metallic melts, σ is Stefan-Boltzmann constant, respectively. T^*, the decay part of the temperature response curve normalized by the maximum temperature rise, T_{max} is approximately represented by the following equation in

the normalized time region between 8 and 12.

$$T^{*} = T_M \exp(-k^{*}) \tag{6}$$

where T_M corresponds to the temperature when extrapolated the attenuation curve down to time at laser beam irradiation. The linear relationship between the logarithmic value of T^{*} and t^{*} may be described as follows.

$$\ln T^{*} = -kt^{*} + 1 \quad T \tag{7}$$

The gradient, k and the intercept, $\ln T_M$, provide information with respect to the effects of radiative and conductive heat loss at interface between melt sample and cell material. The simulated results of the relationship between k and $\ln T_M$ with conduction for the thermal resistance parameter R^{+}, n = 0.5-∞ and Biot number Y = 0 - 0.25 are shown in Fig. 13. This figure includes the experimental results of molten nickel obtained with different conditions and a point at the origin in Fig. 13 corresponds to the adiabatic condition. The experimental results of k and $\ln T_M$ for molten nickel are found to be situated near the curve of $R^{+} = \infty$. Small dispersion is likely to be attributed to the fluctuations in the signal to noise ratio detected in the temperature response curves. Accordingly, the authors maintain the view, from the results of Fig. 13, that the effect of the conductive heat loss at interface between metallic melt and cell material is negligibly small within the present experimental condition. In other words, thermal contact resistance at the interface between molten sample and cell material can be considered to be sufficiently large and consequently only the radiative heat leakage needs to be taken into account for the present experimental condition for the thermal diffusivity measurements.

The thermal diffusivity values of molten iron, cobalt and nickel were measured for iron in the temperature range from 1808 K to 1868 K, for cobalt in the temperature range from 1768 K to 1838 K and for nickel in the temperature range from 1728 K to 1928 K. It may be worth noting that good reproducibility of the experimental thermal diffusivity data was confirmed by repeating the measurements under a given condition more than three times. The results are shown in Fig. 14. Chemical compositions of three metals are summarized in Table 3.

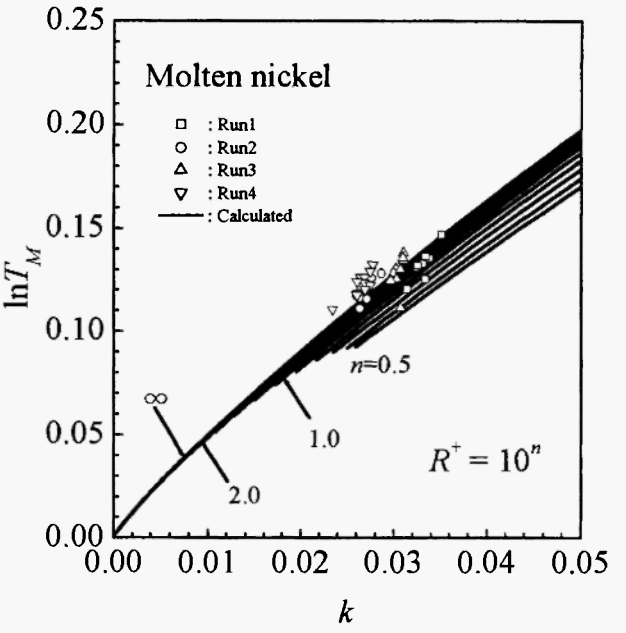

Fig. 13: Relationships between k and $\ln T_M$ of molten nickel. Symbols of □, ○, Δ and ∀ denote the results obtained from the different runs.

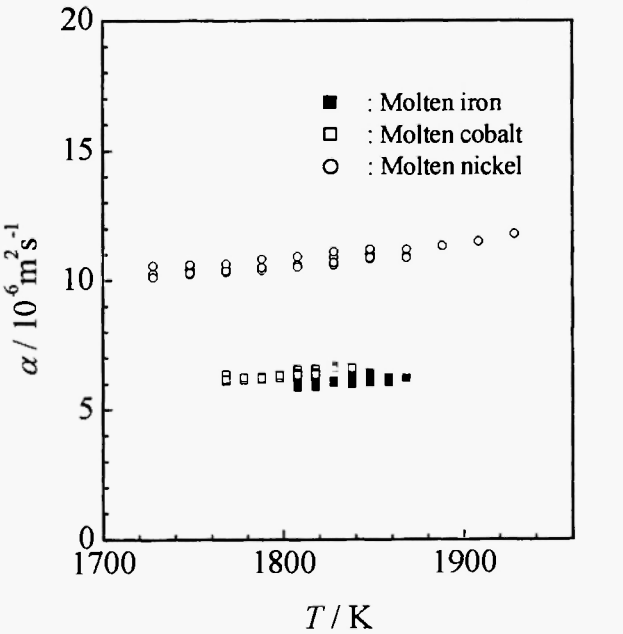

Fig. 14: Thermal diffusivity of molten iron, cobalt and nickel as a function of temperature obtained in this work.

Table 3
Chemical composition (unit: mass%) for iron, cobalt and nickel samples presently investigated.

Chemical composition	Metal		
	Fe	Co	Ni
C	0.018	0.001	<0.01
Si	0.002	–	<0.01
Mn	0.002	<0.00002	0.01
P	0.2	–	0.001
S	0.002	0.0001	<0.001
Fe	--	<0.00006	0.02
Co	–	–	<0.01

The thermal diffusivity value of molten iron at its melting point (1808 K) is 12 % smaller than the reported value of solid iron at 1600 K /2/. For cobalt, with its melting point (1768 K) the liquid value is 21 % smaller than that of solid cobalt at 1700 K and for nickel (with melting point 1728 K) the liquid value is 36 % smaller than that of solid nickel at 1500 K /2/. Such distinct variation in thermal diffusivity of three metals should be related to a change in the structure from the periodic atomic distribution to that with non-periodicity at melting. It is also worth mentioning that the thermal diffusivity values of three metals in the liquid state indicate slightly positive temperature dependence, although the origin of this behavior cannot be certainly identified at the present time.

Thermal diffusivity values of molten three metals are summarized in the following equations (m^2/s) /10/.

$$\begin{aligned} &\alpha_{Fe} = 4.51\times10^{-9}(T-1808)+5.97\times10^{-6} \\ &\quad for\ 1808 < T(\mathrm{K}) < 1868 \\ &\alpha_{Co} = 6.59\times10^{-9}(T-1768)+6.14\times10^{-6} \\ &\quad for\ 1768 < T(\mathrm{K}) < 1838 \\ &\alpha_{Ni} = 6.61\times10^{-9}(T-1728)+1.02\times10^{-5} \\ &\quad for\ 1728 < T(\mathrm{K}) < 1928 \end{aligned} \qquad (8)$$

5. CONCLUDING REMARKS

The current state-of-the-art concerning the laser flash method has been reviewed for determining thermal diffusivity of high temperature oxide and metallic melts.

The values of thermal diffusivity of boron oxide melts and various continuous casting powder melts were successfully obtained by the differential three-layered laser flash method. The effect of radiative component in the cell system on the measured thermal diffusivity was systematically estimated by considering absorption and emission of radiation in the sample layer by using the finite difference method.

Considering the effect of radiative and conductive heat loss at the interface between metallic melt and the cell material, thermal diffusivity values of molten iron, cobalt and nickel at temperature above 1700K were determined with sufficient reliability by the laser flash method.

These results clearly suggest that it would be very promising to extend the laser flash method with a three layered cell to the thermal diffusivity measurements of other melts at high temperature and then its validity and usefulness will be confirmed on a wider base.

REFERENCES

1. K.C. Mills, *Proc. 4th Inter. Conf. on Molten Slag and Fluxes*, Iron Steel Institute of Japan, 1992; p.405.
2. Y.S. Touloukian, C.Y. Ho and P.E. Liley (editors), *Thermophysical Properties of Matter*, Plenum Press, New York, 1971.
3. W.J. Parker, R.J. Jenkins, C.P. Butler and G.L. Abbot, *J. Appl. Phys.*, **32**, 1979(1961).
4. H. Ohta, G. Ogura, Y. Waseda, M. Suzuki and Y.Yamashita, *Rev. Sci. Instrum*, **61**, 2645 (1990).
5. Y. Waseda, M. Masuda and H. Ohta, *Proc. 4th Inter. Symp. on Advanced Nuclear Energy Research*, Japan. Atomic Energy Research Institute, Tokai, Ibaraki, 1992;p.298.
6. G. Ogura, .K. Suh, H. Ohta and Y. Waseda, *J. Ceram. Soc. Japan*, **98**, 320 (1990).
7. Y. Waseda and H. Ohta, *Solid State Ionics*, **22**, 263 (1987).
8. H.M. James, *J. Appl. Phys.*, **51**, 4666 (1980).
9. Y. Waseda, M. Masuda, K. Watanabe, H. Shibata, H. Ohta and K. Nakajima, *High Temp. Mater. Process*, **13**, 267 (1994).

10. T. Nishi, H. Shibata, H. Ohta and Y. Waseda, *Metallur. Trans. A* (2003) in press.
11. T. Nakamura, *Ceramics and Heat*, Gihodo, Tokyo, 1985; p.81.
12. H. Ohta, K. Watanabe, K. Nakajima, H. Shibata and Y. Waseda, *High Temp. Mater. Process*, **12**, 139 (1993).
13. H.Ohta, K.Nakajima, M.Masuda and Y.Waseda, *Proc. 4th Inter. Symp. On Slags and Fluxes*, Iron and Steel Inst. Japan, Tokyo, 1992; p.421.
14. M.I. Darby, *High Temp. High Pressure*, **15**, 629 (1983).
15. E.R. Eckert and R.M. Drake Jr., *Analysis of Heat Transfer*, McGraw-Hill, Kougakusha, Tokyo, 1972; p.254.
16. S. Rosseland, *Theoretical Astrophysics*, Claredon Press, Oxford, 1936; cited in a book of R. Siegel and J.R. Howel, *Thermal Radiation Heat Transfer*, McGraw-Hill, Kougakusha, Tokyo, 1972; p.470.
17. H. Ohta, M. Masuda, K. Watanabe, K. Nakjima, H. Shibata and Y. Waseda, *Tetsu-to-Hagane*, **80**, 463 (1994).